



# Efficient photocatalytic degradation of organic dyes using Fe-doped ZnO nanoparticles

M. Senthil Kumar<sup>1</sup> and C. Arunagiri<sup>2,\*</sup>

<sup>1</sup>Department of Physics, Srinivasan College of Arts and Science, Perambalur 621212, India

<sup>2</sup>PG& Research Department of Physics, Periyar EVR College, Bharathidasan University, Tiruchirappalli 620023, India

Received: 9 March 2021

Accepted: 2 June 2021

Published online:

12 June 2021

© The Author(s), under exclusive licence to Springer Science+Business Media, LLC, part of Springer Nature 2021

## ABSTRACT

ZnO-Fe<sub>x</sub> ( $x = 0, 0.05, 0.075, \text{ and } 0.1$  M) nanoparticles based photocatalysts are successfully synthesized by co-precipitation method. The synthesized nanoparticles are characterized using X-ray diffraction, scanning electron microscopy with energy-dispersive X-ray spectroscopy, and UV-visible double beam spectroscopy techniques. The prepared catalysts and its photocatalytic activity were evaluated by methylene blue and methyl orange dye under UV light irradiation. The effect of various photocatalyst parameters such as pH, catalyst dosage, and initial dye concentration on the photodegradation was examined in detail.

## 1 Introduction

In recent years, many hazardous organic pollutants, such as toxic dyes and organic residuals released into the atmosphere from several industries [1, 2]. The degradation and full-mineralization process are vicious, because of merged structure of organic dyes. Among these organic dyes, methylene blue (MB: C<sub>16</sub>H<sub>18</sub>N<sub>3</sub>SCl) and methyl orange (MO: C<sub>14</sub>H<sub>14</sub>N<sub>3</sub>NaO<sub>3</sub>S) are the most important dyes which are used in textile industries and very harmful to human. Because they cause increased heart rates, cyanosis, shock, sickness, injuries to tissue and various skin infections. They also highly harmful to the atmosphere, which then poses a threat to the health of cattle's and animals [3]. Industrial wastewater treatment and recycling are fundamental objectives to secure the worldwide biological system and improve the environment's

quality. Various techniques have been extensively utilized to suppress pollutants from contaminated water sources [4, 5]. Among them, photocatalysis has emerged to be a promising way to control the massive scale's current environmental pollution. The photocatalysts with semiconducting nanostructures have concerned much more attention due to their exceptional physico-chemical properties in the photocatalytic reaction [6–8].

Many researchers recently developed various photocatalysts using metal oxide semiconductor nanoparticles, including Bi<sub>2</sub>O<sub>3</sub>, TiO<sub>2</sub>, ZnO, and WO<sub>3</sub>. Among these transition metal oxides, zinc oxide (ZnO) is found very sensible in the photocatalytic method due to their wide-bandgap, non-toxicity, and high photosensitivity [9–11]. ZnO is a wide-bandgap semiconductor with a direct energy bandgap ( $E_g \approx 3.37$  eV) [12]. ZnO nanoparticles are especially

Address correspondence to E-mail: arunasuba03@gmail.com

attractive for many interesting nanotechnology applications such as transparent conductive coatings [13], photoanodes for dye-sensitized solar cells (DSSCs) [14], gas sensors [15], and electro-photo luminescent materials [16]. Unfortunately, ZnO can only absorb UV light [17], and photocatalytic degradation efficiency was confined by the electron–hole charge carriers, low-adsorption, and low-reusability. To rectify this problem, numerous reports focused on doping ZnO with transition metal (Fe, Co, Mn) ions [18], non-metal (N, C, S) ions [19], and noble metals loading (Ag, Au, Pd) [20] have been carried out. Wu et al. reported that compared with pure ZnO nanoparticles, ZnO-based materials are potential photocatalysts, that can be used as the scaffold or the coating layer in various heterostructures [21–23].

Various techniques for the synthesis of pure ZnO and Fe-doped ZnO nanoparticles are reported in the literature: hydrothermal method [24], combustion [25], and sol–gel method [26]. Among these synthesis methods, co-precipitation [27] is a flexible method for synthesizing the ZnO nanoparticles due to its low-cost, and easy to operate.

Several studies have been reported that the doping of ZnO with transition metal ions for visible light photocatalysts [28, 29]. It has been discovered that 2% Fe-doped ZnO nanoparticles degraded the methyl orange dye up to 80.8% within 210 min under sunlight irradiation. The Fe-doped ZnO degrades MB in 4 h in sunlight [30]. Zhang et al. investigated that Fe/ZnO nanowires' utilization is superior to P25 against MO [31]. Abbad et al. synthesized a Fe-doped ZnO nanoparticle and degraded 2-chlorophenol under solar irradiation. The most significant photocatalytic action was accomplished with the optimized dopant centralization of 0.5 wt% Fe because of the small crystallite size and low bandgap with a low oxidation–reduction potential [32].

In the present work, we reported the various properties of an efficient Fe-doped ZnO nanoparticles for photocatalytic reaction. The effect various dopant concentration on structural, morphological, optical, and electrical properties of ZnO nanoparticles was investigated. Furthermore, we investigated the photocatalytic degradation of MB and MO dye under UV light irradiation.

## 2 Experimental

### 2.1 Preparation

Fe-doped ZnO (ZnO–Fe<sub>x</sub>) nanoparticles were synthesized using various mol.% ( $x \approx 0, 0.05, 0.075, \text{ and } 0.1$ ) using co-precipitation method. The chemicals such as zinc nitrate hexahydrate [Zn(NO<sub>3</sub>)<sub>2</sub>·6H<sub>2</sub>O], ferric nitrate nonahydrate [Fe(NO<sub>3</sub>)<sub>2</sub>·9H<sub>2</sub>O] and sodium hydroxide [NaOH] used in the present study are of analytical grade obtained from Alfa Aesar chemicals, India.

To synthesis pure ZnO nanoparticles, 10 g of Zn(NO<sub>3</sub>)<sub>2</sub>·6H<sub>2</sub>O was dissolved into 20 mL of deionized water (DW) and in parallel 8 g of NaOH was added drop wise in 100 mL water under continuous stirring until to reach pH 11. Then the above solution was heated in a vacuum oven at 100 °C for 2 h [12]. The obtained precipitates were centrifuged, washed three times with DW and ethanol; finally it was dried at 100 °C for 4 h. The collected precipitates were calcined at 450 °C for 1 h. To synthesis, various concentrations of Fe-doped ZnO nanoparticles, such as Fe = 0.05, 0.075, and 0.1 mol.%, 0.68 to 3.4 g of Fe(NO<sub>3</sub>)<sub>2</sub>·9H<sub>2</sub>O was added into the reaction mixture.

### 2.2 Characterization techniques

XRD patterns of the samples were recorded using a mini desktop X-ray diffractometer (X'PERT PRO MPD) operated at an accelerating potential of 40 kV and 30 mA filament current with CuK $\alpha$  radiation of wavelength 1.5406 Å with a scanning rate of 3/min. (from  $2\theta = 10$  to 80 °C). The surface morphology and particles size of the samples were characterized by scanning electron microscope (SEM-JEOL JS-6390) with energy dispersive X-ray spectrometer (EDS). UV–visible absorbance spectra of the samples were measured with a Systronics: AU-2707 double-beam spectrophotometer in the absorption range 190–1000 nm. Fourier transform infrared (FT-IR) spectra of the samples were analyzed by JASCO FTIR-410 spectrometer in the range 400–4000 cm<sup>-1</sup>. The current–voltage ( $I$ – $V$ ) characteristic curves were recorded using the Keithley electrometer 2400 model.

### 2.3 Photocatalytic degradation test

The photocatalytic activity of the samples was evaluated by the degradation of MB and MO under UV

light irradiation (8 W Philips). 20 mg of ZnO–Fe<sub>x</sub> photocatalysts were dissolved in 20 mL aqueous MB and MO dye solution at various pH (2, 4, and 6). The dye solutions with ZnO–Fe<sub>x</sub> photocatalysts were exposed to UV light from 0 to 180 min. at room temperature. Every 30 min, sampling out 2 ml of dye solution collected from samples for photocatalytic degradation test. The photocatalytic degradation of MB and MO was observed  $\lambda_{\max}$  at  $\sim 664$  and 464 nm respectively using a UV–visible spectrophotometer in the wavelength range 200–800 nm.

### 3 Results and discussion

#### 3.1 X-ray diffraction (XRD)

Figure 1a shows the powder XRD characteristic patterns of ZnO–Fe<sub>x</sub> ( $x \approx 0, 0.05, 0.075, 0.1\%$ ) nanoparticles. All the XRD diffraction peaks are indexed to the hexagonal wurtzite structure of crystalline ZnO, further confirmed from the standard JCPDS No. 36-1451 ( $a = 0.325$  nm and  $c = 0.5207$  nm) [33, 34]. There are no characteristic peaks of Fe phases, or its oxides were not detected in the samples. Figure 1b reveals that the magnification of primary peak at 31.8 (100), 34.3 (002), and 36.3° (101), it shows a minor shift in the 0.05, 0.075, and 0.1% Fe-doped ZnO. The ionic radii of Fe<sup>3+</sup> and Zn<sup>2+</sup> are different (Fe<sup>3+</sup> = 0.68 Å and Zn<sup>2+</sup> = 0.74 Å). This result suggests that the Fe ions substitute into the ZnO lattice [35]. The average crystallite sizes ( $D$ ) of the ZnO–Fe<sub>x</sub> was determined from the Debye–Scherrer equation (Eq. 1) [36].

$$D = \frac{0.9\lambda}{\beta \cos \theta} \quad (1)$$

where  $\lambda$  is the incident of diffraction angle,  $\beta$  is the full width half maximum of the peak (FWHM),  $\theta$  is the wavelength of the X-rays (1.5406 Å), respectively. The lattice parameters and average crystalline size of the samples are listed in Table 1. The average crystallite size ( $D$ ) of ZnO–Fe<sub>x</sub> calculated from XRD data are 23, 21, 16 and 12 nm, respectively. Furthermore, the increasing Fe content reduces the lattice parameters and average crystallite size. Previous reports reported by Jeyachitra et al. [12] in Fe-doped ZnO nanoparticles, Srinivasan et al. [37] in Mn-doped ZnO and Nahm et al. [38] in V<sub>2</sub>O<sub>5</sub>-doped ZnO ceramics are also similar to the obtained results.

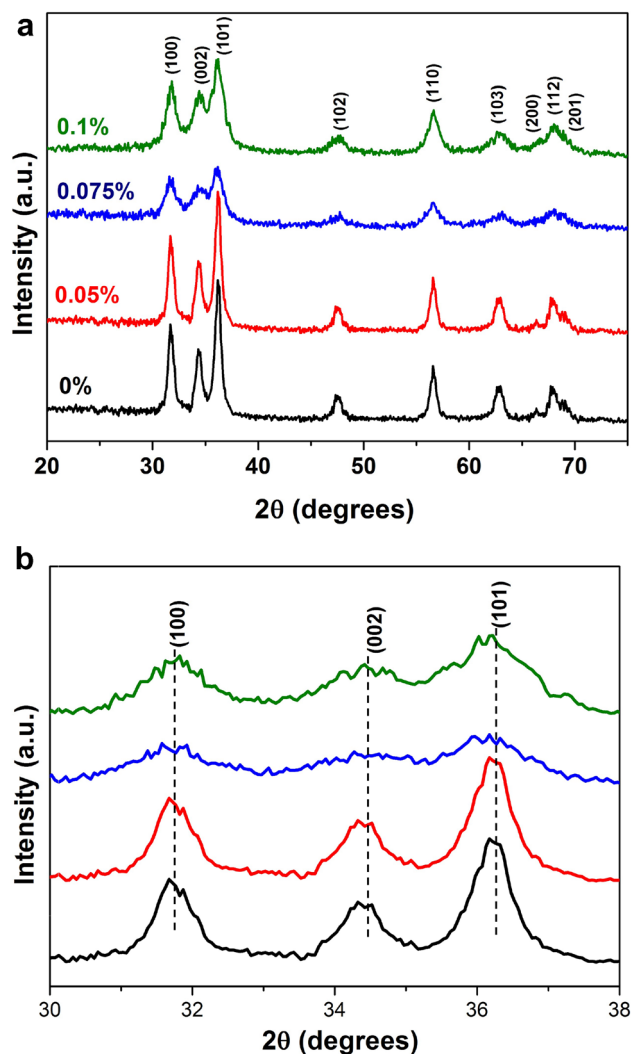


**Fig. 1** XRD patterns of **a** undoped ZnO and Fe-doped ZnO nanoparticles **b** Fe concentration dependent shift in primary diffraction peaks

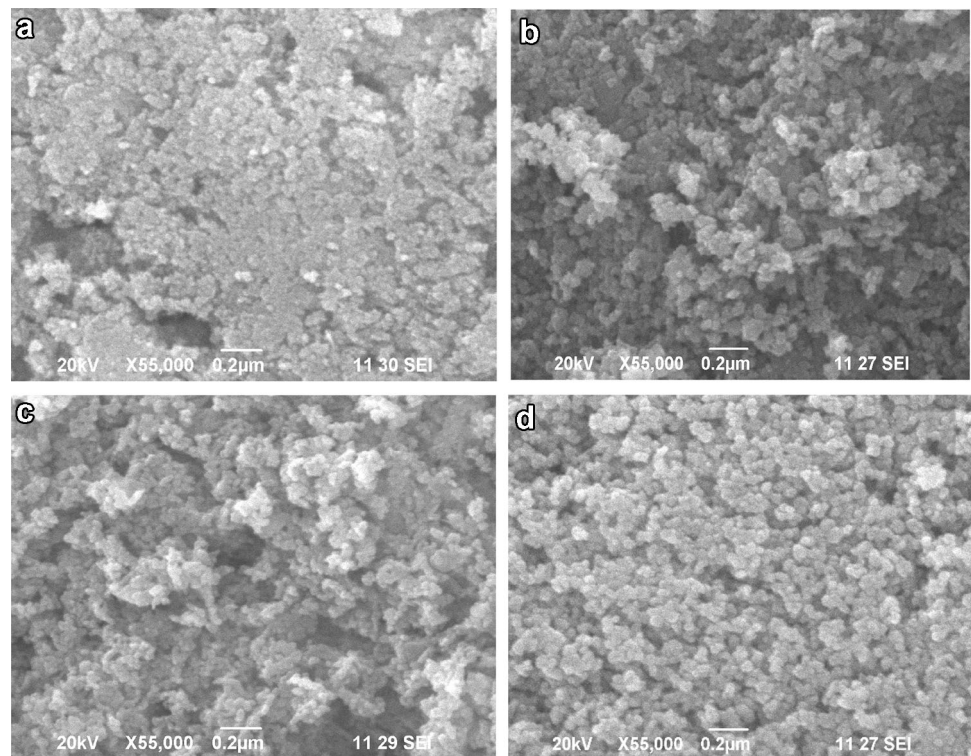
#### 3.2 SEM analysis

The surface morphologies of ZnO–Fe<sub>x</sub> ( $x \approx 0, 0.05, 0.075, \text{ and } 0.1 \text{ mol.}\%$ ) nanoparticles are shown in Fig. 2a–d. Fig. 2a shows the surface morphology of undoped ZnO with crystallite size of  $\sim 42$ –68 nm. Interestingly, when the Fe concentration was 0.05 mol.%, the ZnO nanoparticles are turned and it is shown in Fig. 2b. Figure 2c, d show turning of needle and spherical like structures due to the doping of 0.075 to 0.1 mol.% of Fe-dopants in ZnO nanoparticles. Compared with undoped ZnO, 0.1 mol.% of Fe-doped ZnO shows more information on the surface. The images clearly exposed that the surface morphology changed with the addition of Fe

**Table 1** The lattice parameters and average crystallite size of ZnO–Fe<sub>x</sub> nanoparticles

Fe Doping Concentration (mol.%)	<i>hkl</i>	<i>2θ</i> (degree)	<i>a</i> [Å]	<i>c</i> [Å]	Crystallite size (nm)
ZnO	(100)	31.77	3.24	5.20	23
	(002)	34.40			
	(101)	36.30			
ZnO–Fe <sub>0.05</sub>	(100)	31.81	3.25	5.21	21
	(002)	34.23			
	(101)	36.37			
ZnO–Fe <sub>0.075</sub>	(100)	31.71	3.25	5.20	16
	(002)	34.43			
	(101)	36.17			
ZnO–Fe <sub>0.1</sub>	(100)	31.81	3.24	5.20	12
	(002)	34.23			
	(101)	36.23			

**Fig. 2** SEM images of **a** undoped ZnO **b** 0.05, **c** 0.075 and **d** 0.1 mol.% Fe-doped ZnO nanoparticles



concentration, the agglomerated particles breaks and pores were created and then finally reduced into spherical nanoparticles. It can also be noticed that the size and morphology of ZnO–Fe<sub>x</sub> nanoparticles enhanced with the dopant concentration.

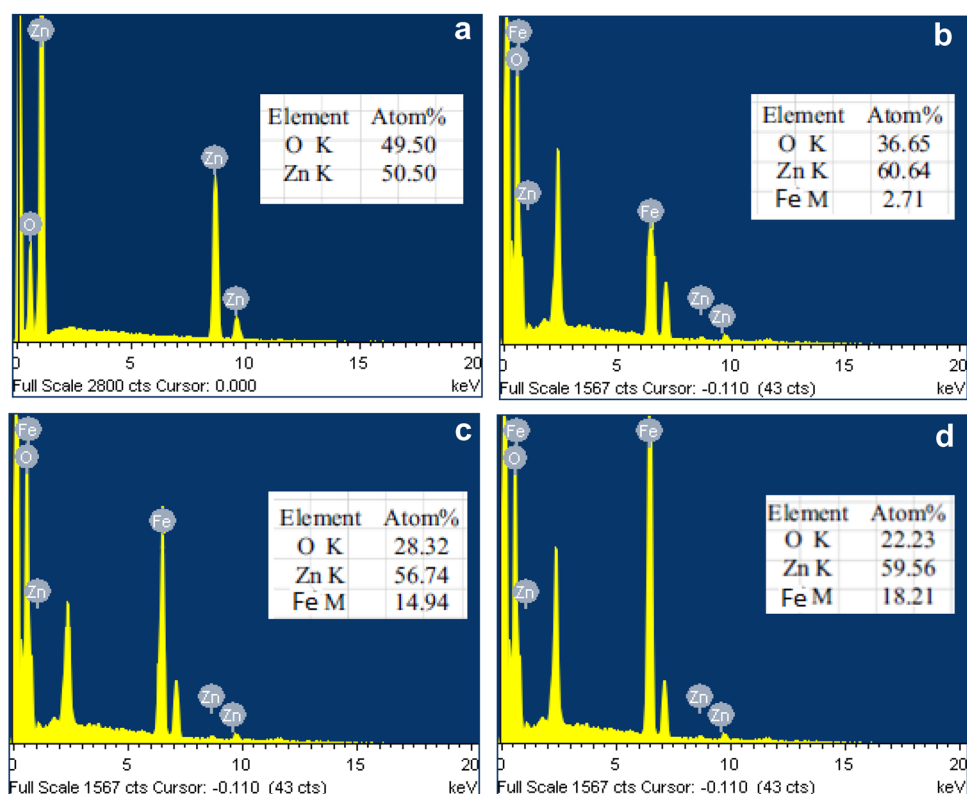
### 3.3 EDX analysis

EDX analysis (Fig. 3a–d) was used to investigate the chemical composition of ZnO–Fe<sub>x</sub> ( $x \approx 0, 0.05, 0.075$  and  $0.1$  mol.%) nanoparticles. EDX spectrum of undoped ZnO shows the existence of characteristic

peaks of oxygen (O) and zinc (Zn) elements (Fig. 3a). The atomic percentage of these elements found to be 49.5 and 50.5%, respectively. Figure 3b–d show the EDX spectra of Fe-doped ZnO nanoparticles also include elements such as O, Zn and Fe, respectively. The inset of EDX image ZnO–Fe<sub>x</sub> nanoparticles data was given in table format. The measured Fe concentration of 0.05, 0.075 and 0.1 mol.%, are about 2.71, 14.94, and 18.21%, respectively. The observed atomic percentage values almost match well with the samples.



**Fig. 3** EDX images of **a** undoped ZnO **b** 0.05, **c** 0.075 and **d** 0.1 mol.% Fe-doped ZnO nanoparticles



### 3.4 UV–Vis spectral studies

UV-absorption spectra of ZnO–Fe<sub>x</sub> ( $x \approx 0, 0.05, 0.075$  &  $0.1$  mol.%) nanoparticles are shown in Fig. 4a–d. The absorption edge is shifted towards a higher wavelength region, which means that the bandgap decreases. The red-shift is due to the increase of crystallite size, and it was confirmed from the XRD results. The optical bandgap of ZnO and Fe-doped ZnO nanoparticles was calculated using the formula  $E_g = hc/\lambda$  [39]. The calculated optical bandgap values are 3.90, 3.89, 3.86 and 3.82 eV, which corresponds to undoped ZnO and 0.05, 0.075 & 0.1 mol.% Fe-doped ZnO nanoparticles. Similar result was also observed by Hassan et al. [40]. The substitute of Fe<sup>3+</sup> with Zn<sup>2+</sup> ion shares the oxygen with Zn atoms and reduces the bandgap.

### 3.5 FTIR analysis

FTIR spectra of ZnO–Fe<sub>x</sub> ( $x \approx 0$  and  $0.1$  mol.%) nanoparticles in the range  $4000$ – $400$  cm<sup>-1</sup> are presented in Fig. 5a, b. The broad absorption band appearing in the range  $3452$ – $3446$  cm<sup>-1</sup> corresponds to –OH stretching vibration, while the two peaks located at  $1625$  and  $1591$  cm<sup>-1</sup> is due to –OH bending

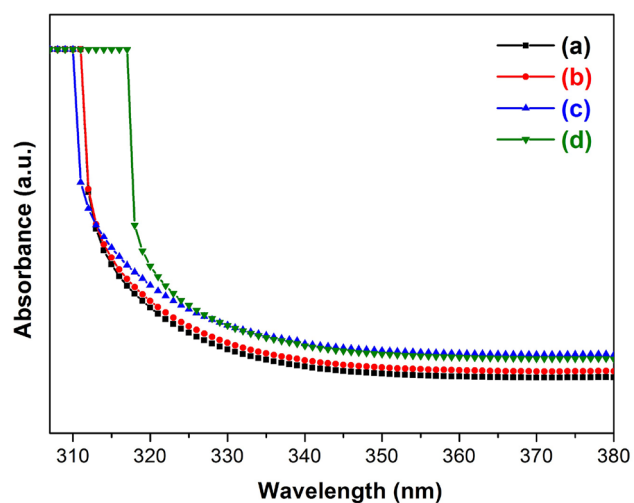


**Fig. 4** UV–Vis absorbance spectra of **a** undoped ZnO **b** 0.05, **c** 0.075 and **d** 0.1 mol.% Fe-doped ZnO nanoparticles

vibration of the adsorbed H<sub>2</sub>O molecules [41]. The band lower intensity absorbed around  $2380$  cm<sup>-1</sup> which corresponds to the symmetric and asymmetric C–H bond. Two weak absorption peaks at  $428$  and  $449$  cm<sup>-1</sup> for undoped and  $0.1$  mol.% Fe-doped ZnO sample may corresponds to Zn–O stretching mode. The absorption peaks located at  $1120$ ,  $1122$ , and

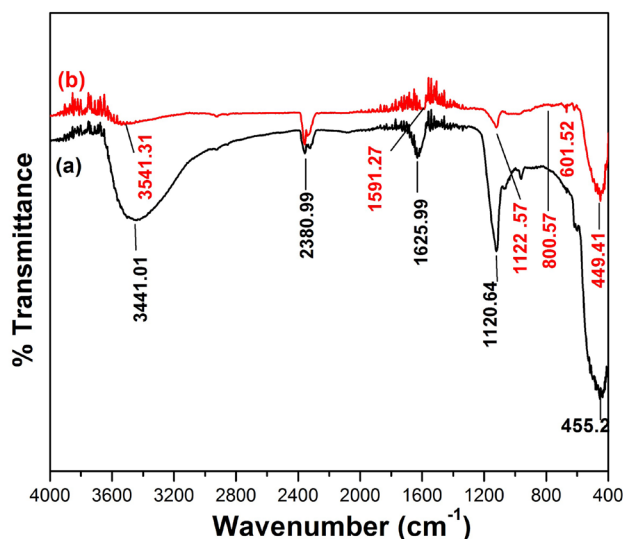


**Fig. 5** FT-IR spectra of **a** undoped ZnO and **b** 0.1 mol.% Fe-doped ZnO nanoparticles

800  $\text{cm}^{-1}$  attributed to the sulfate group, respectively [42]. Also, FTIR spectra of 0.1 mol.% Fe-doped ZnO shows that the small stretch observed at 601  $\text{cm}^{-1}$  corresponds to Fe–O stretch, as reported by Liu et al. [42]. Therefore, it might be due to  $\text{Fe}^{3+}$  ions substituted in Zn.

### 3.6 *I*–*V* characteristics

The *I*–*V* characteristics of  $\text{ZnO-Fe}_x$  ( $x \approx 0$  and 0.1 mol.%) nanoparticles have been determined using Ag-paste for better electrical contact and the result is shown in Fig. 6a, b. From these curves, DC electrical conductivity measurement of  $\text{ZnO-Fe}_x$  ( $x \approx 0$  and 0.1 mol.%) nanoparticles taken under varying temperatures of 30, 50, 70, 90, 110 and 130 °C (Increase of 20 °C). Thus, it increases the conductivity of 0.1 mol.% Fe-doped ZnO nanoparticles due to the increase in the mobility of charge carriers [43]. The remarkable increase in these samples conductivity may result in a higher advantage for optical device fabrication.

### 3.7 Photodegradation of MB and MO

#### 3.7.1 Influence of pH

The adsorption of MB and MO dye molecules on undoped ZnO nanoparticles strongly depends on the solution's pH displayed in Fig. 7a. The influence of pH on the photodegradation of MB and MO dye was

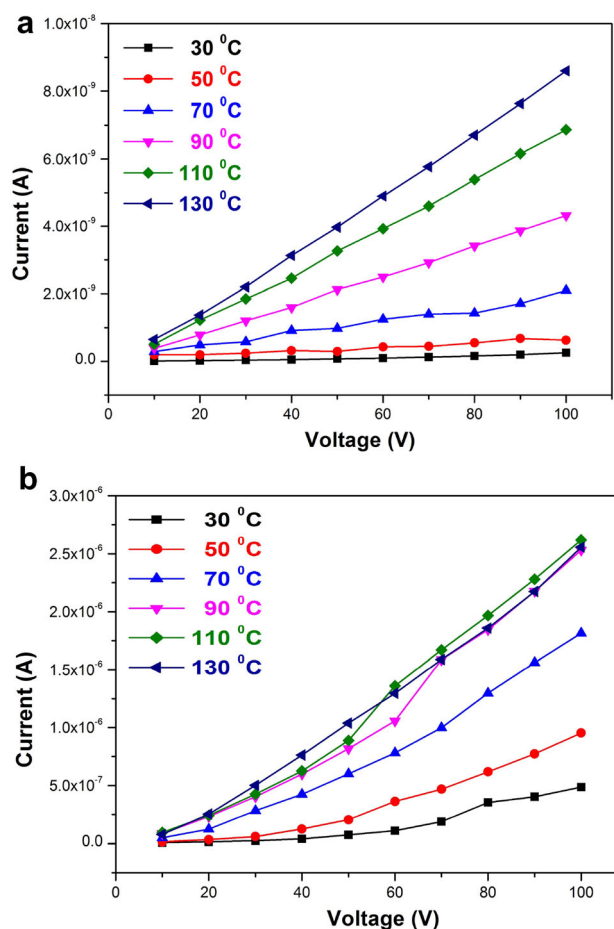


**Fig. 6** *I*–*V* characteristics of **a** undoped ZnO and **b** 0.1 mol.% Fe-doped ZnO nanoparticles

studied by varying the solution's pH from 2 to 6. The outcome shows that photodegradation was maximum in base medium. The degradation arrives at most extreme at pH 6 and decreases sensibly up to pH 2. Henceforth, the pH 6 was accepted as an ideal pH and utilized for additional investigation.

#### 3.7.2 Influence of catalyst concentration

The influence of catalyst concentration on the photodegradation of MB and MO dye was verified using ZnO catalyst concentrations from 5 to 15 mg/30 ml in 10 ppm MB, and MO dye solution at pH 6 and it is displayed in Fig. 7b. The variation in photodegradation can be clarified by accessibility of several surface-active sites and UV light radiation into dye solution. The photodegradation reaches maximum at 10 mg/30 ml. The reduced photodegradation at higher catalyst concentration (15 mg/30 ml) may be

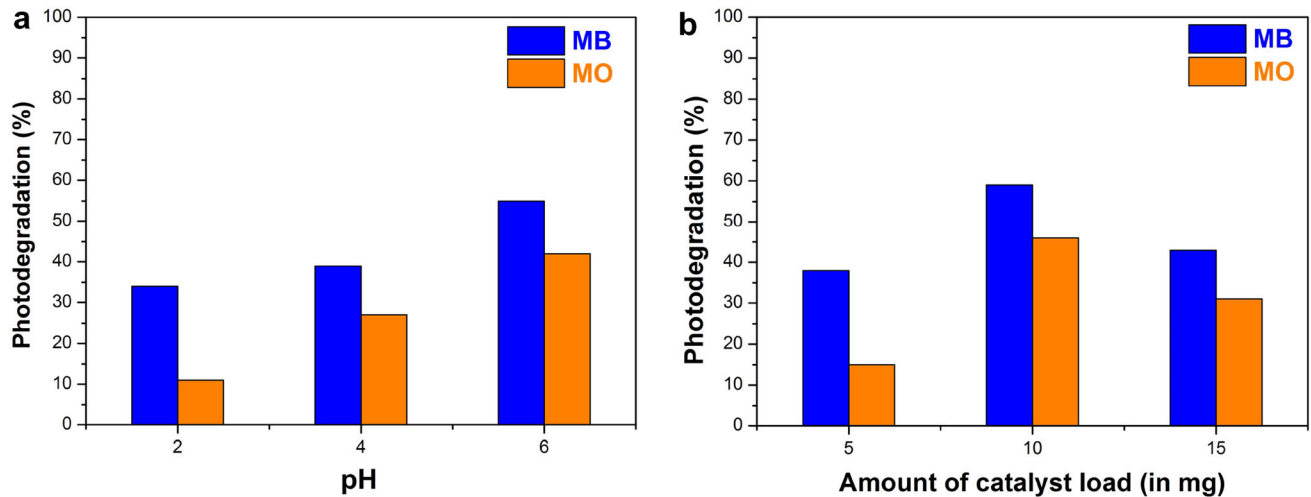


**Fig. 7** **a** Influence of pH and **b** catalyst concentration on the photodegradation of MB and MO

due to ZnO nanoparticles aggregation increases the scattering effect [44]. Consequently, 10 mg/30 ml ZnO photocatalyst was expected as an ideal catalyst weight.

### 3.7.3 Influence of UV irradiation time of MB

The photocatalytic activity was carried out with MB concentration of 2.0 mM, catalyst concentration of 10 mg, pH 6 and irradiation time up to 150 min. Figure 8a–d show the variation in absorption spectra of MB illuminated to UV light for various irradiation times (0, 30, 60, 90, 120 and 150 min) in the presence of ZnO–Fe<sub>x</sub> ( $x \approx 0, 0.05, 0.075, 0.1$  mol.%) nanoparticles. The intensity of absorption peaks at 664 nm decreases gradually with irradiation time.

MB dye was degraded under UV light from 0 to 150 min. in the presence of ZnO–Fe<sub>x</sub> ( $x \approx 0, 0.05, 0.075, 0.1$  mol.%) nanoparticles and is shown in Fig. 8e. The result reveals that the Fe-doped ZnO shows higher photocatalytic activity than that of undoped ZnO. Fe (0.075%)-doped ZnO shows enhanced photocatalytic activity with a degradation efficiency of 68% for MB (pH 6) dye at 150 min. Fe (0.075%)-doped ZnO nanoparticles took less time to degrade the MB dye compared with other concentration of Fe. The reduction of photocatalytic activity at higher concentration Fe (0.1%)-doped ZnO may be due to photons' reduced path length [44]. Similar results are also observed by Suganthi and colleagues [45]. Another reason for the increase in the photocatalytic activity of Fe-doped ZnO nanoparticles, Fe ions substituted into ZnO surface may suppress the

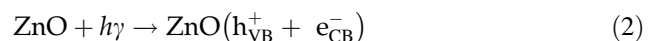
electron–hole pair recombination and enhance the dye degradation efficiency [46, 47].

### 3.7.4 Influence of UV irradiation time of MO

The photocatalytic activity was carried out with MO concentration of 3.0 mM, catalyst concentration of 10 mg, pH 6 and irradiation time up to 150 min. The variation in absorption spectra of MO showing to UV light for various irradiation times (0, 30, 60, 90, 120 and 150 min) in the presence of ZnO–Fe<sub>x</sub> ( $x \approx 0, 0.05, 0.075, 0.1$  mol.%) nanoparticles. The intensity of absorption peaks at 454 nm decreases gradually with the extension of irradiation time shown in Fig. 9a–d.

Figure 9e shows the MO dye degradation under UV light from 0 to 150 min. in the presence of ZnO–Fe<sub>x</sub> ( $x \approx 0, 0.05, 0.075, 0.1$  mol.%) nanoparticles. The result reveals that the Fe (0.075%)-doped ZnO showed efficient photocatalytic activity with a degradation efficiency of 55% for MO (pH 6) dye at 150 min [48].

In this process, narrow semiconductors act as a sensitizer to improve the dye's photodegradation based on their electronic band structure. When the photocatalyst was illuminated with higher energy photons, it only allows the dye molecule oxidation [44]. We proposed a mechanism of ZnO–Fe<sub>x</sub> nanoparticles for efficient photocatalytic activity. It can be described as follows:



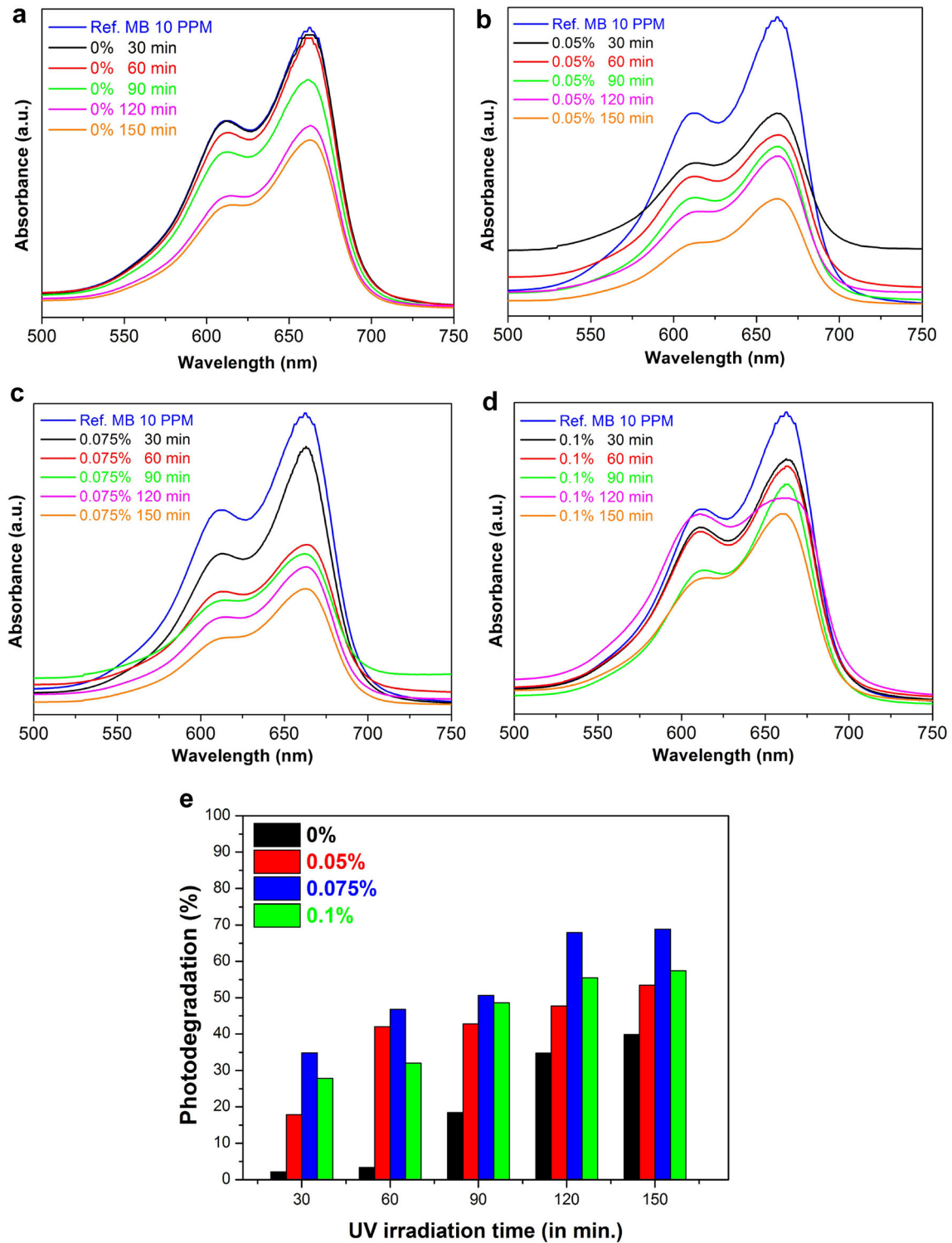


**Fig. 8** UV-Vis absorption spectra of MB dye degradation of **a** undoped ZnO **b** 0.05, **c** 0.075, and **d** 0.1 mol.% Fe-doped ZnO nanoparticles and **e** influence on the photodegradation of MB



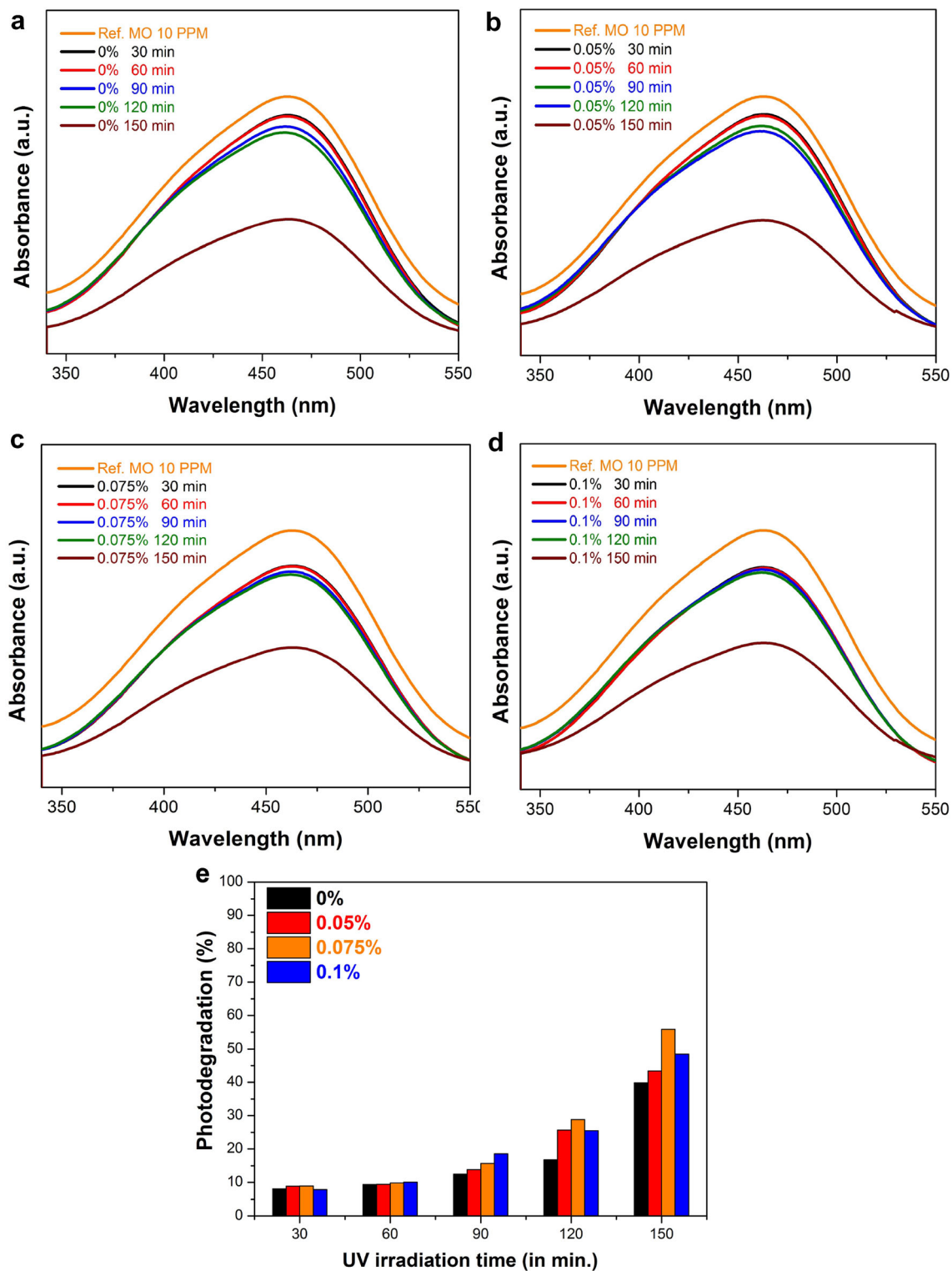
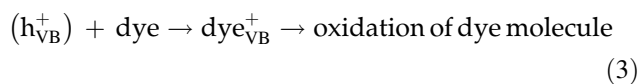
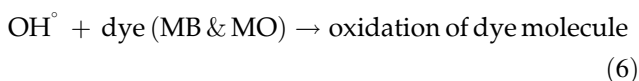
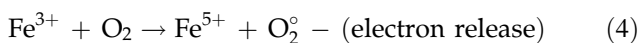


**Fig. 9** UV–Vis absorption spectra of MO dye degradation of **a** undoped ZnO **b** 0.05, **c** 0.075, and **d** 0.1 mol.% Fe-doped ZnO nanoparticles and **e** influence on the photodegradation of MO



When ZnO is illuminated by visible light, holes ( $h_{\text{VB}}^+$ ) and electrons ( $e_{\text{CB}}^-$ ) are generated and passed through from valence to conduction band. The photogenerated electrons and holes combine with  $\text{Fe}^{3+}$  ions, respectively.



These superoxide anions ( $\text{O}_2^{\circ-}$ ) and hydroxyl radicals ( $\text{OH}^\circ$ ) are strong oxidizing species, and it will degrade of MB and MO dye molecule (Eq. 6) [48]. From these results, novel Fe-doped ZnO nanoparticles have played a primary role in the degradation of organic dyes from wastewater.

## 4 Conclusion

In this paper, we reported the synthesis of ZnO- $\text{Fe}_x$  ( $x \approx 0, 0.05, 0.075$  &  $0.1$  mol.%) nanoparticles by coprecipitation method. The intensity of Fe-doped ZnO nanoparticles decreases due to the incorporation of Fe ( $0.05, 0.075$  &  $0.1$  mol.%), confirmed by XRD. Doping of Fe modifies the morphology and crystallite size of ZnO nanoparticles and it was estimated to be  $\sim 42$ – $68$  nm. UV-Vis absorbance studies reveals that increasing of Fe concentration up to  $0.1$  mol.%, the bandgap decreases when compared with undoped ZnO. The maximum percentage of MB and MO photodegradation was achieved for the dosage concentration of  $10$  mg and irradiation time of  $150$  min at pH  $6$ . Fe-doped ZnO nanoparticles may be used as an efficient photocatalyst to degrade the organic dyes under UV light.

## References

1. A. Nezamzadeh-Ejhi, N. Moazzeni, *J. Ind. Eng. Chem.* **19**, 1433–1442 (2013)
2. M. Safari, M. Nikazar, M. Dadvar, *J. Ind. Eng. Chem.* **19**, 1697–1702 (2013)
3. A. Arques, A.M. Amat, A. Garcia-Ripoll, R. Vicente, *J. Hazard. Mater.* **146**, 447 (2007)
4. V.K. Gupta, D. Pathania, S. Agarwal, P. Singh, *J. Hazard. Mater.* **243**, 179 (2012)
5. B.K. Korbahti, K. Artut, C. Gecgel, A. Ozer, *Chem. Eng. J.* **173**, 677 (2011)
6. J.B. Joo, I. Lee, M. Dahl, G.D. Moon, F. Zaera, Y. Yin, *Adv. Funct. Mater.* **23**, 4246–4254 (2013)
7. T.H. Yu, W.Y. Cheng, K.J. Chao, S.Y. Lu, *Nanoscale* **5**, 7356 (2013)
8. M. Lima, D. Fernandes, M. Silva, M. Baesso, A. Neto, G. de Moraes et al., *J. Sol-Gel Sci. Technol.* **72**, 301–309 (2014)
9. B. Cao, W. Cai, *J. Phys. Chem. C* **112**, 680 (2008)
10. R. Saravanan, M.M. Khan, V.K. Gupta, E. Mosquera, F. Gracia, V. Narayanan, A. Stephen, *RSC Adv.* **5**, 34645–34651 (2015)
11. R. Saravanan, N. Karthikeyan, V.K. Gupta, E. Thirumal, P. Thangadurai, V. Narayanan, A. Stephen, *Mater. Sci. Eng., C* **33**, 2235–2244 (2013)
12. R. Jeyachitra, V. Senthilnathan, T.S. Senthil, *J Mater Sci. Mater Electron* **29**, 1189–1197 (2018)
13. D. Rajesh, B. Varalakshmi, C.S. Sunandana, *Phys. B* **407**, 4537–4539 (2012)
14. M. Arshad, M.M. Ansari, A.S. Ahmed, P. Tripathi, S.S.Z. Ashraf, A.H. Naqvi, A. Azam, *J. Lumin.* **161**, 275e280 (2015)
15. L. Chow, O. Lupan, G. Chai, H. Khallaf, L.K. Ono, B.R. Cuenya, I.M. Tiginyan, V.V. Ursaki, V. Sontea, A. Schulte, *Sens. Actuators A* **189**, 399–408 (2013)
16. Y.X. Liua, Y.C. Liua, D.Z. Shena, G.Z. Zhonga, X.W. Fana, X.G. Konga, R. Muc, D.O. Hendersonc, *J. Cryst. Growth* **240**, 152–156 (2002)
17. T. Bak, J. Nowotny, M. Rekas, C. Sorrell, *Int. J. Hydr. Energy* **27**, 991–1022 (2002)
18. Z. Han, L. Ren, Z. Cui, C. Chen, H. Pan, J. Chen, *Appl. Catal. B Environ.* **126**, 298 (2012)
19. S.S. Shinde, C.H. Bhosale, K.Y. Rajundoped, *J. Photochem. Photobiol. B* **113**, 70 (2012)
20. Y. Min, K. Zhang, Y. Chen, Y. Zhang, W. Zhao, *Sep. Purif. Technol.* **92**, 115 (2012)
21. H. Wu, Z. Zheng, Y. Tang, N.M. Huang, R. Amal, H.N. Lim, Y.H. Ng, Pulsed electrodeposition of CdS on ZnO nanorods for highly sensitive photoelectrochemical sensing of copper (II) ions. *Sustain. Mater. Technol.* **18**, e00075 (2018)
22. H. Wu, Z. Zheng, C.Y. Toe, X. Wen, J.N. Hart, R. Amal, Y.H. Ng, *J. Mater. Chem. A* **8**, 5638–5646 (2020)
23. H. Wu, T.H. Tan, R. Liu, H.-Y. Hsu, Y.H. Ng, *Sol. RRL* (2021). <https://doi.org/10.1002/solr.202000423>
24. A. Moulahi, F. Sediri, *Ceram. Int.* **40**, 943–950 (2014)

25. N.L. Tarwal, P.R. Jadhav, S.A. Vanalakar, S.S. Kalagi, R.C. Pawar, J.S. Shaikh et al., *Powder Technol.* **208**, 185–188 (2011)
26. T. Ivanova, A. Harizanova, T. Koutzarova, B. Vertruyen, *Mater. Lett.* **64**, 1147–1149 (2010)
27. A. Rahmati, A.B. Sirgani, M. Molaei, M. Karimipour, *Eur. Phys. J. Plus* **129**, 7 (2014)
28. P. Malathy, K. Vignesh, M. Rajarajan, A. Suganthi, *Ceram. Int.* **40**, 101 (2014)
29. B.M. Rajbongshi, S.K. Samdarshi, *Appl. Catal. B: Environ.* **144**, 435 (2014)
30. S. Dong, K. Xu, J. Liu, H. Cui, *Phys. B* **406**, 3609 (2011)
31. Y. Zhang, M.K. Ram, E.K. Stefanalkos, D.Y. Goswami, *Surf. Coat. Technol.* **217**, 119 (2013)
32. M.M. Ba-Abbad, A.A.H. Kadhum, A. Mohamad, M.S. Takriff, K. Sopian, *Chemosphere* **91**, 1604–1611 (2013)
33. A.A. Ashkarran, A. Irajizad, S.M. Mahdavi, M.M. Ahadian, *Mater. Chem. Phys.* **118**, 6–8 (2009)
34. J. Zhou, F. Zhao, Y. Wang, Y. Zhang, L. Yang, *J. Lumin.* **122–123**, 195–197 (2007)
35. S. Bai, T. Guo, Y. Zhao, J. Sun, D. Li, A. Chen et al., *Sens. Actuators B Chem.* **195**, 657–666 (2014)
36. M. Nasir, S. Bagwasi, Y. Jiao, F. Chen, B. Tian, J. Zhang, *Chem. Eng. J.* **236**, 388 (2014)
37. G. Srinivasan, J. Kumar, *Cryst. Growth* **310**, 1841 (2008)
38. C.W. Nahm, *J. Mater. Sci. Mater. Electron.* **24**, 70 (2013)
39. T.G. Venkatesh, Y.A. Nayaka, R. Viswanatha, C.C. Vidyasagar, B.K. Chethana, *Power Tech.* **225**, 232–238 (2012)
40. M.M. Hassan, W. Khan, A. Azam, A.H. Naqvi, *J. Ind. Eng. Chem.* **21**, 283–291 (2015)
41. A. Mesaros, C.D. Ghitulica, M. Popa, R. Mereu, A. Popa, T. Petrisor Jr., M. Gabor, A.I. Cadis, B.S. Vasile, *Ceram. Int.* **40**, 2835–2846 (2014)
42. C. Liu, D. Meng, H. Pang, X. Wua, J. Xie, X. Yu, L. Chen, X. Liu, *J. Magn. Magn. Mater.* **324**, 3356 (2012)
43. S. Abed, H. Bougharraf, K. Bouchouit, Z. Sofiani, B. Derkowska-Zielinska, M.S. Aida, B. Sahraoui, *Superlattice Microstruct.* **85**, 370 (2015)
44. S.V. Elangovan, V. Chandramohan, N. Sivakumar, T.S. Senthil, *Desalin. Water Treat.* **57**, 9671–9678 (2016)
45. K. Vignesh, M. Rajarajan, A. Suganthi, *J. Ind. Eng. Chem.* **20**, 3826–3833 (2014)
46. W. Bousslama, H. Elhouichet, M. Ferid, *Optik* **134**, 88 (2017)
47. X. Yu, D. Meng, C. Li, U.K. Xu, J. Chen, C. Lu, Y. Wang, *J. Mater. Sci.* **25**, 3920 (2014)
48. S.K. Kansal, M. Singh, D. Sud, *J. Hazard. Mater.* **141**, 581–590 (2007)

**Publisher's Note** Springer Nature remains neutral with regard to jurisdictional claims in published maps and institutional affiliations.